Constraint-Aware Null-Space Inverse Kinematics for a 9-DOF Mobile Manipulator

Tadele Belay Tuli*[1], Abubakar Mughal[1] and Martin Manns[1]

***Abstract*— Mobile manipulators play crucial role in industrial automation to combine mobility and manipulation in flexible environment. However, operational space control of such robots is not trivial. This paper presents a constraint-aware differential inverse kinematics solver for a 9-DOF mobile manipulator arm. The method combines damped least-squares regularisation, null-space projection, and smooth joint-limit weighting with feasibility-preserving saturation to enforce strict mechanical limits throughout motion execution. The proposed method is validated in simulation demonstrating an improvement in mechanically safe solution rate across a structured shelf workspace. A sensitivity analysis identifies a critical stability boundary in the null-space gain parameter, providing a quantitative tuning criterion for redundancy-based controllers. The results establish that kinematic redundancy can be systematically exploited for joint-limit avoidance and safe motion generation in constrained industrial manipulation tasks.**

NOMENCLATURE

Symbol	Description
Kinematics	
n	Number of joints (degrees of freedom)
$\mathbf{q} \in \mathbb{R}^n$	Joint configuration vector
$\dot{\mathbf{q}} \in \mathbb{R}^n$	Joint velocity vector
$\mathbf{q}_{\min}$, $\mathbf{q}_{\max}$	Lower and upper joint limit vectors
$\mathbf{x} \in \mathbb{R}^m$	End-effector pose in task space
$\dot{\mathbf{x}} \in \mathbb{R}^m$	End-effector velocity
$T \in SE(3)$	Homogeneous transformation matrix
$M \in SE(3)$	End-effector home configuration
Jacobian and Inverse Kinematics	
$\mathbf{J} \in \mathbb{R}^{m\times n}$	Geometric Jacobian matrix
$\mathbf{J}^+$	Moore–Penrose pseudoinverse of $\mathbf{J}$
$\mathbf{J}^+_\lambda$	Damped least-squares (DLS) pseudoinverse of $\mathbf{J}$
λ	Damping factor for DLS regularization
$\mathbf{P} = \mathbf{I} - \mathbf{J}^+_\lambda \mathbf{J}$	Null-space projection matrix
k	Null-space gain for secondary objective
$\mathbf{q}_0$	Secondary objective vector (e.g., joint centering)
$\mathbf{V}_s \in \mathbb{R}^6$	End-effector twist in space frame
ϵ_ω, ϵ_v	Convergence tolerances (angular, linear)
Performance Metrics	
w	Manipulability index, $w = \sqrt{\det(\mathbf{J}\mathbf{J}^\top)}$
e	End-effector position error [mm]
Screw Theory	
$\mathcal{S}_i \in \mathbb{R}^6$	Screw axis of joint i in space frame
$[\mathcal{S}_i]$	Matrix representation of screw axis $\mathcal{S}_i$
Ad_T	Adjoint transformation associated with $T \in SE(3)$

I. INTRODUCTION

In modern industrial automation, mobile manipulators that integrate locomotion with robotic arms are emerging as key enablers of flexible and adaptive production systems (cf. [1]). By combining mobility and manipulation, these systems extend the operational workspace beyond the limitations of fixed-base robots, enabling autonomous task execution across spatially distributed environments.

This capability enhances production flexibility by supporting dynamic reconfiguration and a wide range of tasks, thereby facilitating scalable and modular automation architectures [2]. However, the integration of mobile manipulators into existing industrial systems introduces new challenges in control, coordination, and scalability, which remain barrier to their widespread adoption in next-generation smart factories.

In this work, a laboratory demonstrator, the SkaLaB production cell for sheet metal car body parts [3], is considered. The system employs a redundant mobile manipulator to support scalable manufacturing concepts in human-centered production environments. The manipulator consists of a 7-DOF robotic arm mounted on a mobile base, augmented with an additional revolute base joint and a prismatic vertical lift axis, resulting in a 9-degree-of-freedom (9-DOF) kinematic chain (R-P-R-R-R-R-R-R-R, where R is revolute, and P is prismatic joint). While this redundancy enhances reachability and flexibility, it significantly increases the complexity of motion control due to the nonlinearity and underdetermined nature of the inverse kinematics problem.

Analytical inverse kinematics (IK) solutions are computationally efficient but are only applicable to specific kinematic structures [4]. In contrast, numerical IK approaches, such as Newton–Raphson or pseudoinverse-based methods, are more general and can be applied to arbitrary kinematic chains [5]. However, these methods typically prioritize minimization of end-effector error while neglecting physical constraints [6], [7].

As a result, such approaches may generate configurations that lead to collisions involving multiple system components, including the manipulator, mobile base, shelves, and auxiliary tooling systems. A critical limitation arises from the prismatic lift joint, which is physically bounded by the mobile base structure. During lower position tasks, such as reaching Shelf 4 at $z = 0.097\,\mathrm{m}$ (cf. fig. 1), conventional IK solvers often fail to ensure collision-free motion. Although these methods may converge numerically, their feasibility deteriorates significantly in constrained workspace regions, with safe solution rates dropping to as low as 11% in the worst-case scenario. This reveals a fundamental mismatch between mathematical feasibility and physical realizability in high-redundancy robotic systems.

To address this issue, a constraint-aware inverse kinematics approach is required that actively exploits redundancy

[1] PROTECH - Institut für Produktionstechnik, Universität Siegen, Siegen, Germany
*tadele-belay.tuli@uni-siegen.de

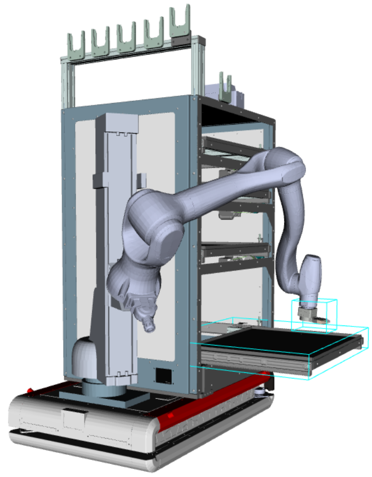

Fig. 1. 9-DOF mobile manipulator visualized in RViz.

to redistribute motion when joints approach their limits, while maintaining accurate end-effector positioning. Such an approach enables safe operation by resolving the inherent trade-off between task accuracy and collision-free execution.

II. Related Work

The evolution of industrial robotics has progressed from fixed, highly structured automation toward flexible and mobile systems characteristic of Industry 4.0 (cf.[1]). Traditional manipulators, typically fixed-base and optimized for repetitive tasks, are increasingly supplemented by mobile manipulators that combine robotic arms with autonomous platforms [6], [8]. This integration extends the operational workspace beyond the physical reach of a single manipulator, enabling complex tasks such as distributed assembly and warehouse logistics [9].

A defining characteristic of mobile manipulators is kinematic redundancy. A system is considered redundant when its degrees of freedom exceed the dimensionality of the task space. For typical manipulation tasks requiring six degrees of freedom, a 9-DOF system provides additional flexibility that can be exploited for secondary objectives such as obstacle avoidance, singularity avoidance, and joint limit handling [5]. This capability, often referred to as self-motion, allows the robot to maintain the end-effector pose while reconfiguring its internal structure [10].

The hardware platform considered in this work introduces heterogeneous joint types, which pose additional challenges for inverse kinematics due to differences in units and scaling between translational and rotational joints. These differences can affect numerical stability in Jacobian-based methods.

Kinematic modeling of robotic systems is traditionally performed using the Denavit–Hartenberg (DH) convention [6]. While effective for simple serial chains, DH becomes less intuitive for redundant systems, particularly when dealing with mixed joint types or near-parallel axes. As an alternative, the Product of Exponentials (PoE) formulation, based on screw theory, provides a global and coordinate-free representation of robot kinematics [5]. In this formulation, each joint (θ_n) is modeled as a screw axis (S_n), and the forward kinematics is expressed as:

$$T_{sb}(\mathbf{q}) = e^{[\mathcal{S}_1]\, q_1}\, e^{[\mathcal{S}_2]\, q_2}\, \dots\, e^{[\mathcal{S}_n]\, q_n}\, M \tag{1}$$

The inverse kinematics (IK) problem for redundant manipulators is inherently non-linear and underdetermined, often yielding infinitely many solutions [6]. Analytical solutions are limited to specific kinematic structures and are generally not applicable to high-DOF systems [4]. Consequently, numerical methods are widely adopted due to their general applicability.

Among numerical approaches, the Newton–Raphson method and its variants rely on iterative updates derived from the Jacobian matrix (J). For redundant systems, the Moore–Penrose pseudoinverse provides a minimum-norm solution:

$$\dot{\theta} = J^{+}\dot{x} = J^{T}(JJ^{T})^{-1}\dot{x} \tag{2}$$

This formulation computes the smallest joint velocity vector that achieves the desired end-effector motion. However, it assumes that the matrix (JJ^T) is well-conditioned. Near kinematic singularities, (JJ^T) becomes ill-conditioned or non-invertible, resulting in unbounded joint velocities and unstable motion [11], [12]. Furthermore, the pseudoinverse formulation does not incorporate any mechanism for handling joint limits or physical constraints.

To address numerical instability, the Damped Least Squares (DLS) method introduces a regularization term, resulting in a damped pseudoinverse:

$$J_{\lambda}^{+} = J^{T}(JJ^{T} + \lambda^{2}I)^{-1} \tag{3}$$

The damping factor λ ensures that the matrix $(JJ^T + \lambda^2 I)$ remains invertible even near singular configurations. As a result, joint velocities remain bounded and numerically stable. This approach can be interpreted as a regularized version of the pseudoinverse, trading small tracking errors for improved robustness.

Redundancy can be exploited through null-space projection [13], which allows secondary objectives to be incorporated without affecting the primary task. In this formulation, the primary task is defined as tracking the desired end-effector motion $\dot{x}$, while the secondary objective $\dot{q}_0$ influences the internal configuration of the robot:

$$\dot{\theta} = J_{\lambda}^{+}\dot{x} + (I - J_{\lambda}^{+}J)\dot{q}_0 \tag{4}$$

The first term $(J_{\lambda}^{+}\dot{x})$ ensures convergence of the end-effector to the desired pose, while the second term lies in the null-space of the Jacobian and does not affect the end-effector motion. The secondary objective $(I - J_{\lambda}^{+}J)$ is commonly used for joint centering or constraint avoidance for redundant manipulators [13]. However, null-space projection provides only a soft constraint and does not strictly guarantee that joint limits will not be violated.

To enforce joint feasibility, saturation and weighting-based constraint handling strategies have been introduced. These approaches ensure that joint values remain within physical limits by restricting updates during each iteration [10]. Combining null-space projection for proactive avoidance with feasibility-preserving constraint handling enables reliable operation in constrained environments. Despite these advancements, many existing implementations rely on generic or black-box solvers, limiting transparency and customization. This motivates the development of a dedicated, constraint-aware inverse kinematics method tailored for high-DOF mobile manipulators.

III. Objective

The objective of this work is to develop and validate a robust differential inverse kinematics (IK) solver for a 9-DOF mobile manipulator (see fig. 1) that ensures strict adherence to mechanical constraints while maintaining high positioning accuracy. This work contributes to a method based on a differential inverse kinematic solver that ensures joint-limit compliance and safe operation in constrained environments combining damped least squares, null-space projection, and smooth joint-limit weighting. This allows to actively redistribute motion across available degrees of freedom when constraints are encountered. This involves identification of a critical gain boundary for stable solver behavior, multi-stage validation including workspace sampling, testing, and dynamic tracking.

IV. Method

This section presents a differential inverse kinematics method that systematically integrates established methods into a unified, constraint-aware solver tailored for high-redundancy systems operating under strict physical constraints. The key contribution lies in combining differential IK with smooth constraint handling and redundancy-driven motion reallocation, enabling safe operation in constrained industrial environments.

A. Kinematic Modeling

The system kinematics follows the Product of Exponentials formulation (cf. Eq. 1), providing a consistent representation of the manipulator configuration. Each joint is expressed as a screw axis $S_i = (\omega_i, v_i)$, where ω_i defines the axis direction and v_i defines the linear component. The forward kinematics parameters for Eq. 1 are given in table I.

TABLE I

Screw Axis Parameters of the 9-DOF Mobile Manipulator

Joint	ω_i	v_i	Description
1	$(0,0,1)$	$(0,0,0)$	Base
2	$(0,0,0)$	$(0,0,1)$	Lift
3	$(-0.707,0,0.707)$	$(-0.007,0.155,-0.007)$	Shoulder 1
4	$(0,-1,0)$	$(0.551,0,0.770)$	Shoulder 2
5	$(-0.707,0,0.707)$	$(-0.008,0.151,-0.008)$	Elbow 1
6	$(0,-1,0)$	$(1.049,0,1.267)$	Elbow 2
7	$(-0.707,0,0.707)$	$(-0.009,0.154,-0.009)$	Wrist 1
8	$(0,-1,0)$	$(1.537,0,1.757)$	Wrist 2
9	$(-0.707,0,0.707)$	$(-0.012,0.154,-0.012)$	Wrist 3

Zero-configuration frame M:

$$M = \begin{bmatrix} 0.707 & 0 & -0.707 & -1.881 \\ 0 & 1 & 0 & -0.012 \\ 0.707 & 0 & 0.707 & 1.663 \\ 0 & 0 & 0 & 1 \end{bmatrix}$$

The relationship between joint velocities and end-effector motion is given by:

$$V_s = J_s(\theta)\dot{\theta} \tag{5}$$

where V_s denotes the spatial twist and $J_s(\theta)$ is the configuration-dependent Jacobian.

B. Constraint-Aware IK Solver

To address these limitations, a Gradient Projection (GP) based method integrating three components: DLS, null-space projection, and explicit constraint handling is proposed.

1) Damped Least Squares: The damped pseudoinverse (cf. [11], [12] given in Eq. 3) is used to ensure numerical stability near singularities.

2) Null-Space Projection: Redundancy is resolved using the classical gradient projection approach proposed by [10] in Eq. 4. The secondary objective is defined as joint centering:

$$q_0 = k\left(\frac{q_{max} + q_{min}}{2} - \theta\right) \tag{6}$$

where k is the centering gain.

3) Constraint Handling: To maintain joint feasibility while avoiding abrupt transitions near joint limits, a smooth joint-limit weighting strategy is incorporated into the inverse kinematics update. The weighting progressively reduces the contribution of joints approaching their limits and redistributes motion through the redundant degrees of freedom. As a final safety mechanism, a clipping operation is applied:

$$\theta_i = \begin{cases} q_{i,max}, & \theta_i > q_{max} \\ q_{i,min}, & \theta_i < q_{min} \\ \theta_i, & \text{otherwise} \end{cases} \tag{7}$$

As a joint approaches its limit, the null-space component progressively redistributes motion across the remaining degrees of freedom, allowing continued task execution without violating constraints. The joint update is computed as:

$$\theta_{k+1} = \theta_k + J^+ V_s + (I - J^+ J) q_0 \tag{8}$$

This process is repeated until convergence while continuously adapting the joint weighting and enforcing feasibility at each iteration. The solver configuration is summarized in Table II.

TABLE II

Solver Parameters

Parameter	Value	Unit
Tolerance	10^{-3}	m
Max Iterations	150	–
Damping λ	0.01	–
Gain k	0.05–0.15	–
Time Step	0.01	s

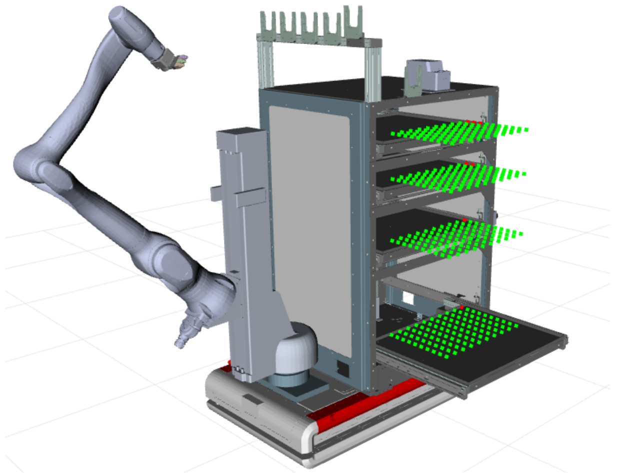

Fig. 2. Workspace validation through numerical convergence and mechanical safety across shelf levels (displayed in Rviz, red points indicate no solution).

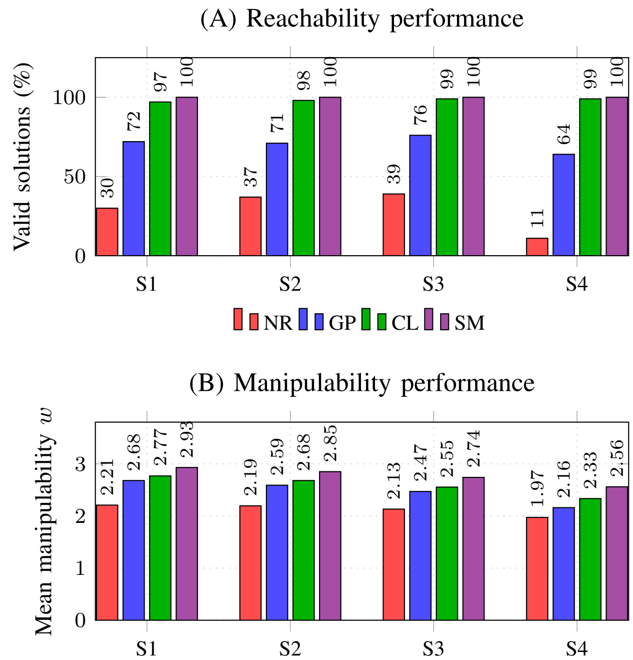

Fig. 3. Comparison of inverse kinematics methods across four shelf levels. (A) Percentage of targets yielding valid joint-limit compliant solutions. (B) Mean manipulability index at the converged solution. NR: Newton–Raphson, GP: Gradient Projection, CL: GP with hard clamping, SM: GP with smooth weighting (proposed).

V. Experimental Design

A multi-stage validation step is designed to evaluate solver performance under varying levels of constraint and redundancy interaction.

1) *Workspace Validation* - A total of 400 target points are sampled across four shelf levels to evaluate global reliability. This test quantifies the difference between numerical convergence and mechanical feasibility.
2) *Redundancy Reallocation* - A forced failure scenario is constructed by commanding the end-effector to a position requiring violation of the prismatic joint limit. The solver's ability to redistribute motion across redundant joints is evaluated.
3) *Gain Sensitivity* - This identifies the stability region in which null-space projection improves safety without degrading convergence.
4) *Dynamic Trajectory Tracking* - A 3D sine-wave trajectory is used to evaluate continuous motion behavior.

VI. Results

In this section, the proposed constraint-aware inverse kinematics solver is evaluated across four experimental criteria: workspace coverage, end-effector accuracy, redundancy reallocation, and sensitivity to null-space gain. All results are compared against a Newton–Raphson pseudoinverse solver (NR), GP, GP with Clamping (CL) and GP with smooth weighting (SM).

A. Workspace Validation

Global workspace coverage was assessed over a 10×10 Cartesian grid at each of the four shelf levels, yielding 400 IK queries per solver (see fig. 2). In fig. 3(A), the collision safe rate of the Newton-Raphson falls to 11 % at Shelf 4 ($z = 0.097$ m), confirming that the majority of its solutions violate joint limits and are physically inadmissible. Gradient projection (GP), which augments the same damped pseudoinverse with null-space centering but no explicit limit enforcement, raises the valid rate to 64–76% yet still admits a substantial fraction of violations, showing that soft centering expresses a preference for mid-range postures rather than a hard constraint. The hard-clamping formulation (CL) maintains a consistent safe solution rate of 97–99 % across all shelf levels, whereas the proposed smooth weighting formulation (SM) achieves 100 % safe feasible solutions over the entire workspace.

The mean manipulability index $w = \sqrt{\det(\mathbf{J}\mathbf{J}^\top)}$ (fig. 3(B)) improves from 2.21 (NR) to 2.93 (SM) at Shelf 1, and from 1.97 to 2.56 at Shelf 4. Compared with hard clamping, the smooth weighting formulation consistently achieves higher manipulability while preserving joint-limit compliance.

B. Redundancy Reallocation

A trajectory-level evaluation was conducted on the lowest shelf, representing the most constrained workspace region. As shown in fig. 4(A), the Newton–Raphson solver violates the lower prismatic joint limit throughout the entire trajectory. Both CL and SM maintain strict feasibility.

The manipulability evolution shown in fig. 4(B) indicates that the constraint-aware methods exploit redundancy more effectively than NR. While both constrained methods improve dexterity, the smooth weighting strategy achieves the highest manipulability over the entire trajectory (mean $w = 2.77$) compared to the Newton-Raphson (mean $w = 2.125$), a gain of approximately 23 %, confirming that constraint enforcement actively improves the mechanical quality of the solution rather than merely restricting it. .

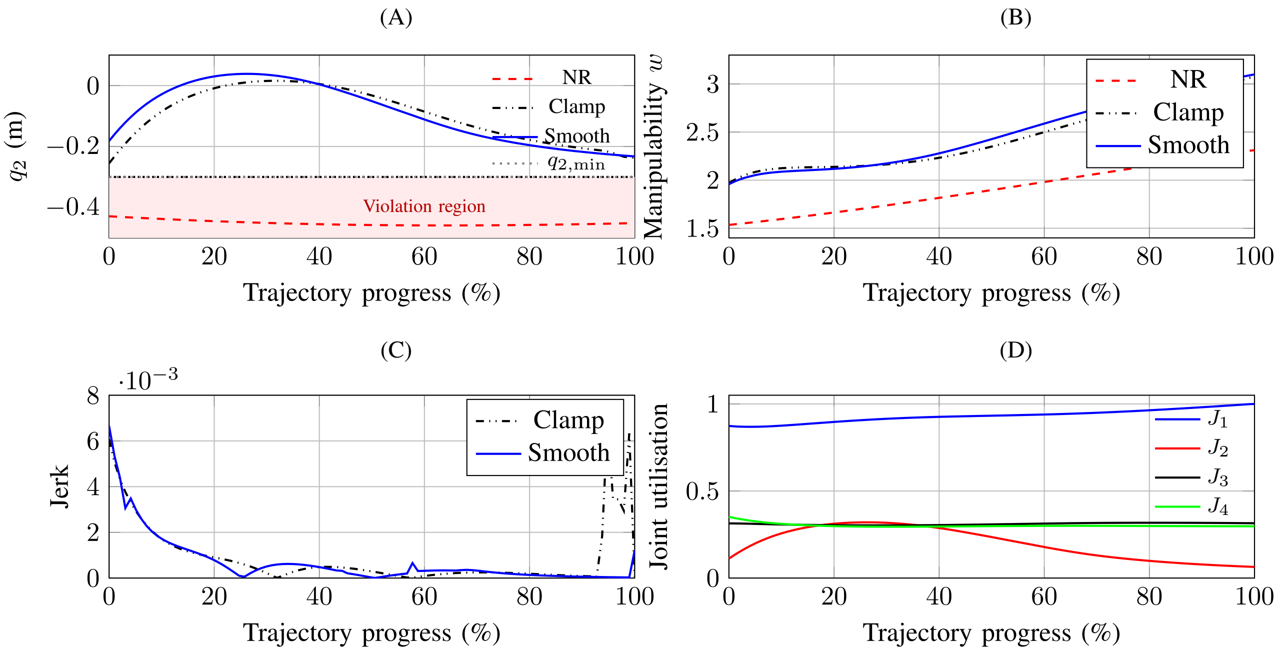

Fig. 4. Trajectory-level comparison for the low-shelf scenario. (A) Evolution of the prismatic base joint q_2. (B) Manipulability evolution along the trajectory. (C) Jerk comparison between hard clipping and the proposed smooth weighting formulation. (D) Normalized joint utilisation for the Smooth method, illustrating effective exploitation of the available configuration space while maintaining feasibility.

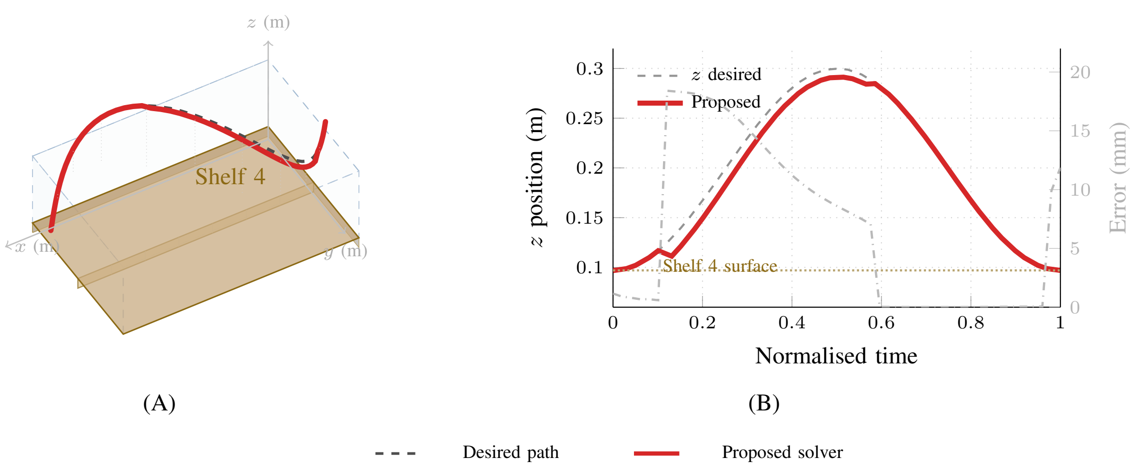

Fig. 5. Sinusoidal end-effector trajectory within the bounding volume of Shelf 4 (sliced view). Drop lines project the end effector (EE) onto the shelf surface. Black dashed: desired path. Red solid: proposed solver.

Figure 4(C) highlights the key difference between CL and SM. Although hard clamping enforces feasibility, it introduces abrupt changes in the null-space motion, resulting in distinct jerk spikes near joint-limit activation. The proposed smooth weighting formulation significantly attenuates these spikes and produces a more continuous trajectory. This confirms that smooth constraint handling improves motion quality without sacrificing workspace coverage or manipulability. Figure 4(D) presents the normalized joint utilization of the proposed solver for J_1–J_4. Initially, all joints contribute to task execution, with J_2 providing the dominant vertical reach. As J_2 approaches its lower limit, the weighting function progressively reduces its contribution and redistributes the motion toward J_3 and J_4.

C. Sensitivity to Null-Space Gain

The influence of the null-space gain parameter k on solver performance was evaluated by sweeping $k \in [0.0, 2.0]$ at uniform increments. As shown in table III, for $k \leq 0.8$, the solver maintains full convergence and safety compliance across all test targets. Within this range, the secondary objective effectively biases the solution toward the joint-space center without interfering with primary task convergence. For $k \geq 1.5$, the solver fails to converge entirely on constrained targets. This behavior identifies $k \in (0.1, 0.8]$ as the practical stability region and provides actionable guidance for gain selection in deployment.

TABLE III

EFFECT OF NULL-SPACE GAIN k ON SOLVER PERFORMANCE ACROSS THE SHELF WORKSPACE (400 QUERIES PER VALUE).

k	Success rate (%)	Safe rate (%)	Mean w
0.05	100.0	97.3	2.71
0.10	100.0	97.8	2.74
0.30	100.0	98.1	2.79
0.50	100.0	97.9	2.76
0.80	100.0	97.2	2.68
1.00	84.3	61.4	2.31
1.50	12.7	9.8	1.87
2.00	0.0	0.0	—

D. Dynamic Trajectory Tracking

As shown in fig. 5, a transient tracking error of approximately 18.6 mm was observed. This deviation results from the solver prioritizing joint-limit compliance while continuously redistributing motion through the redundant degrees of freedom. The error subsequently decreases as the remaining joints compensate for the constrained motion and restore task alignment. The observed error therefore represents a practical trade-off between constraint satisfaction and tracking performance in highly constrained workspace regions.

VII. DISCUSSION AND CONCLUSION

Results reveal that numerical convergence alone is an insufficient criterion for evaluating IK solvers in constrained redundant systems. While the Newton-Raphson (NR) solver converges for a subset of target poses, its success rate deteriorates significantly in constrained workspace regions. The proposed SM method addresses this by embedding constraint awareness directly into the IK update law through the combination of damped least-squares regularisation, null-space projection, and smooth joint-limit weighting. This formulation preserves task accuracy while handling mechanical feasibility at constraint boundaries.

A key finding is the constructive role of kinematic redundancy. The 3 DOF redundancy of the nine-joint system provides a non-trivial null space that the secondary objective exploits to redistribute motion across the shoulder and elbow joints as the prismatic lift approaches its lower bound. The consistent manipulability improvement observed across all shelf levels indicates that redundancy is exploited not only to avoid constraint violations but also to guide the robot toward kinematically favourable configurations.

The identification of a stability boundary at $k \approx 1.0$ provides a quantitative design criterion for selecting null-space gain, complementing the qualitative guidance typically found in the literature. Trajectory-level analysis further highlights the difference between hard clamping and smooth weighting. Although both approaches maintain joint-limit feasibility, hard clamping introduces abrupt changes in the null-space motion when a joint reaches its limit. The proposed smooth weighting formulation redistributes motion progressively across the redundant joints, resulting in reduced jerk and a more continuous transition between unconstrained and constrained configurations. This behaviour improves motion quality without sacrificing workspace coverage or manipulability.

In future work, first, velocity and acceleration constraints will be incorporated into the inverse kinematics solver to prevent rapid postural shifts during null-space compensation, which can exceed motor controller limits in physical deployment. Second, a closed-loop feedback loop between the IK solver and path planner will be investigated, enabling proactive trajectory modification when the solver detects sustained limit saturation, thereby eliminating error spikes before they occur. Physical deployment in a lab environment and digital twinning are the immediate next steps, during which the sim-to-real transfer of the validated solver will be evaluated under real sensor noise, payload variation, and communication latency.

ACKNOWLEDGMENT

The authors would like to acknowledge the financial support from the DFG within the HiSMoT project (grant number: 500490184).

REFERENCES

[1] N. Ghodsian, K. Benfriha, A. Olabi, V. Gopinath, and A. Arnou, "Mobile Manipulators in Industry 4.0: A Review of Developments for Industrial Applications," *Sensors*, vol. 23, no. 19, p. 8026, Jan. 2023.

[2] Z. Arkouli, G. Kokotinis, G. Michalos, N. Dimitropoulos, and S. Makris, "AI-enhanced cooperating robots for reconfigurable manufacturing of large parts," *IFAC-PapersOnLine*, vol. 54, no. 1, pp. 617–622, Jan. 2021.

[3] M. Schiller, P. Frohn-Sörensen, F. Schreiber, D. Morez, M. Manns, and B. Engel, "Smart design and additive manufacturing of bending tools to improve production flexibility," *Manufacturing Letters*, vol. 41, pp. 91–102, Oct. 2024.

[4] D. L. Pieper, "The kinematics of manipulators under computer control," Ph.D. dissertation, Stanford University, Department of Computer Science, 1968.

[5] K. M. Lynch and F. C. Park, *Modern Robotics: Mechanics, Planning, and Control*. Cambridge University Press, 2017.

[6] B. Siciliano, L. Sciavicco, L. Villani, and G. Oriolo, *Robotics: Modelling, Planning and Control*. Springer, 2009.

[7] S. Toritani, R. L. A. Shauri, K. Nonami, and D. Fujiwara, "Numerical Solution Using Nonlinear Least-Squares Method for Inverse Kinematics Calculation of Redundant Manipulators," *Journal of Robotics and Mechatronics*, vol. 24, no. 2, pp. 363–371, Apr. 2012.

[8] A. Hentout, M. Hamadouche, A. Maoudj, and C. Yalaoui, "Mobile multi-robot systems: A survey on coordination and control," *Journal of Intelligent & Robotic Systems*, vol. 96, pp. 569–594, 2019.

[9] O. Khatib, "A unified approach for motion and force control of robot manipulators: The operational space formulation," *IEEE Journal on Robotics and Automation*, vol. 3, no. 1, pp. 43–53, 1987.

[10] A. Liégeois, "Automatic supervisory control of the configuration and behavior of multibody mechanisms," *IEEE Transactions on Systems, Man, and Cybernetics*, vol. 7, no. 12, pp. 868–871, 1977.

[11] C. W. Wampler, "Manipulator inverse kinematic solutions based on vector formulations and damped least-squares methods," *IEEE Transactions on Systems, Man, and Cybernetics*, vol. 16, no. 1, pp. 93–101, 1986.

[12] S. R. Buss, "Introduction to inverse kinematics with Jacobian transpose, pseudoinverse and damped least squares methods," University of California, San Diego, Tech. Rep., 2004. [Online]. Available: https://mathweb.ucsd.edu/ sbuss/ResearchWeb/ikmethods/iksurvey.pdf

[13] Y. Nakamura, H. Hanafusa, and T. Yoshikawa, "Task-priority based redundancy control of robot manipulators," *The International Journal of Robotics Research*, vol. 6, no. 2, pp. 3–15, 1987.